We are IntechOpen,
the world's leading publisher of
Open Access books
Built by scientists, for scientists

6,900
Open access books available

186,000
International authors and editors

200M
Downloads

154
Countries delivered to

Our authors are among the

TOP 1%
most cited scientists

12.2%
Contributors from top 500 universities

CLARIVATE ANALYTICS

BOOK
CITATION
INDEX

INDEXED

WEB OF SCIENCE™

Selection of our books indexed in the Book Citation Index
in Web of Science™ Core Collection (BKCI)

Interested in publishing with us?
Contact book.department@intechopen.com

Numbers displayed above are based on latest data collected.
For more information visit www.intechopen.com

Development of Novel Polymer Nanostructures and Nanoscale Complex Hydrides for Reversible Hydrogen Storage

Sesha S. Srinivasan and Prakash C. Sharma

Additional information is available at the end of the chapter

1. Introduction

This book chapter discusses about (i) the characteristics of hydrogen – a clean and renewable fuel, (ii) the grand challenges in hydrogen storage in reversible solid state hydrides, the current technical targets set forth by the US Department of Energy and the FreedomCAR, (iii) current state of hydrogen storage (Broom, 2011), (iv) various types of hydrogen storage methods and modes (Bowman & Stetson, 2010; Sathyapal et. al., 2007). Among the different methods of hydrogen storage, the current book chapter aims to address two important hydrogen storage methods such as physisorbed hydrogen storage via polymer nanostructures and chemisorbed hydrogen storage via complex chemical hydrides. The experimental approaches of synthesizing the solid state hydrides using mechanochemical milling, wet chemical synthesis and electrospinning are discussed. Extensive metrological characterization techniques such X-ray diffraction (XRD), Scanning Electron Microscopy (SEM), Fourier Transform Infrared Spectroscopy (FTIR), Differential Scanning Calorimetry (DSC), Thermogravimetric Analysis (TGA), Thermal Programmed Desorption (TPD), Pressure-Composition-Temperature Isotherms (PCT) are employed to unravel the structural, microstructural, chemical, thermal and volumetric behavior of these materials. The major results based on the structure-property relations are discussed in detail. In summary, a comparative study of various solid state hydrides investigated for reversible hydrogen storage are discussed with potential hydrogen fuel cell applications.

As traditional fossil fuel supplies are dwindling and carbon emissions derived from burning these fuels are being blamed for global weather changes, it is becoming increasingly important to find alternative energy sources. While there are clean and renewable energy production methods, such as wind and solar energy, there is yet to be found a clean and safe

means of propelling automobiles. Hydrogen is an ideal candidate since it can easily be refueled in automobiles similar to gasoline. Its onboard storage, however, is a significant barrier for utilizing hydrogen as a fuel. The materials developed as part of this present study provides a significant improvement in the hydrogen storage properties of solid state storage (Jena, 2011).

Two main approaches are investigated as part of this current investigation. The first is to tailor the nanostructure of polyaniline in its emeraldine form, a conductive polymer, so that the surface area of the polymer is increased, by creating nanospheres and nanofibers. The bulk form of polyaniline is also investigated for its hydrogen sorption properties as a comparison. The reason behind using a polymer for hydrogen storage is that polymers contain many hydrogen atoms which allow for the formation of weak secondary bonds between the hydrogen that is part of the polymer and the hydrogen that is meant to be stored. Since polyaniline is easily synthesized and is rather inexpensive, it is an excellent choice as a hydrogen storage material. The alteration of the physical structure of polyaniline into nanospheres and nanofibers allows for an increase in surface area, thereby exposing more material as potential bonding sites for the hydrogen. However, as host materials of hydrogen physical adsorption, it has a weak interaction (quadrupole interaction) with nonpolar hydrogen molecule. Therefore, some positive ions such as Li+ can be added in quinoid and benzenoid to enhance interaction strength. The Lithium doped polymer electrode is recently shown to exhibit higher ionic conductivity (2×10^{-4} S cm^{-1}) at room temperature in addition to its greater charge-discharge cycles at room temperature (Nitanii et. al., 2005; Zhang et. al., 2012). The photoelectron spectroscopic studies and quantum chemical calculations revealed the role of lithium in the polyaniline systems thus enhances the charge transfer; highly localized and energetically favored at N-atomic sites for the bonding of dimers of N-atoms with the Li-atoms (Kuritka et. al., 2006). Moreover, the insertion of Li$^+$ in the polymer structure affects the electrochemical properties due to their strong interaction with the quinoid and benzenoid rings (Lindino et. al., 2012).

Since polyaniline is composed of quinoid and benzenoid rings and the emeraldine form is terminated with Cl$^-$ ions, additional hydrogen bonding sites, in the form of stronger chemisorption of hydrogen, is made available. The advantage of having both chemisorption and physisorption sites is shown schematically in Figure 1.

Hydrogen, as a molecule, can bond to the material through three main mechanisms. The simplest form is to simply bond weakly to the host material via physisorption as a molecule. This can generally be achieved if the temperature is low enough, and is the main mechanism of storage for physisorption materials, but generally requires temperatures of approximately 77K. If additive materials, such as catalysts, are present, these materials can break up the molecule into ions which then allows for the diffusion through the relatively porous material to then chemically bond with the host material. It is inevitably demonstrated that the vital role of catalyst species such as Ti, Fe, Ni, Pd etc. thus enhances the physico-chemical adsorption of hydrogen atoms on the polyaniline matrices (Skowron´ski & Urbaniak, 2008; Yildirim & Ciraci, 2005). Similarly, hydrogen molecules can also bond the host material. By increasing the surface area as well as the porosity, two main events can occur.
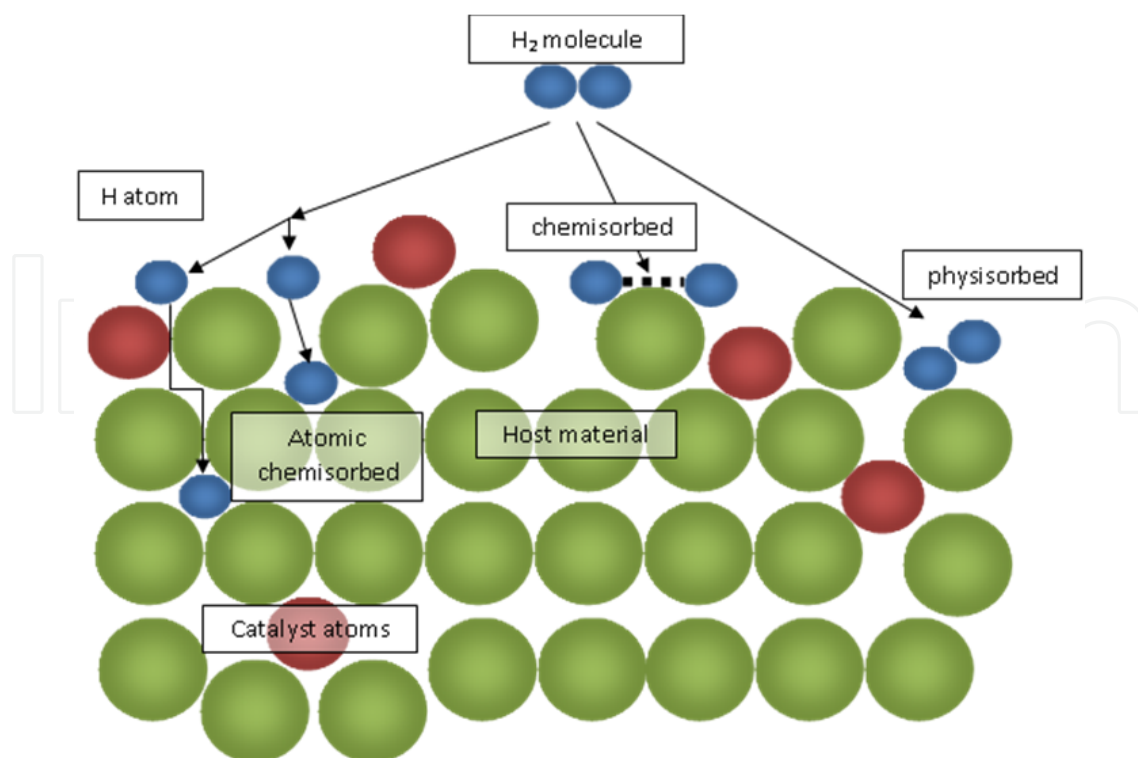
Figure 1. Schematic representation of physisorption and chemisorption with catalyst materials.

The first is that the hydrogen has more bonding sites to the host material. The second is that the diffusion of hydrogen into the material is made possible. Since polyaniline cannot be simply modified to have smaller molecular size, the nanostructure can be altered to increase the surface area and also to increase the hydrogen diffusion pathways. Recently, polyaniline is shown to possess outstanding hydrogen storage properties by carefully modifying the nanostructure of the material. It is found that polyaniline combines both physisorption as well as chemisorption for storing hydrogen, which provides a significant improvement of hydrogen storage properties, since a usable capacity is achieved.

The second mechanism investigated as part of this study is the route of chemisorption, or strong hydrogen atomic bonding, to complex hydride materials. Complex hydrides generally require a high temperature for hydrogen release as the hydrogen bonds are very strong. By reducing the crystallite size of the host material, specifically $LiBH_4$ and $LiNH_4$ and by further destabilizing the structure with MgH_2, the temperature can be reduced to allow for reversible hydrogen storage at a lower temperature (Srinivasan et. al., 2012). The reduction of crystallite size, as well as the exact processing technique is shown to be very important and have a large effect on the storage capacity. Figure 2 shows general hydrogen absorption and desorption of complex hydrides.

The unhydrided material absorbs hydrogen from the outside until it is fully charged with hydrogen. By reducing the pressure on the sample or by increasing the temperature, the hydrogen is then released from the outside first until the material is fully discharged again. When the particles are too large, though, a hydrogen passivation layer can form during the initial hydrogen uptake, thereby reducing any further hydrogenation. Additionally, the

kinetics, or rate, of hydrogen sorption is increased with particle size, as this means that the hydrogen has a larger distance to diffuse through.

The effects of particle size on hydrogen storage are shown in Figure 3. By employing mechano chemical milling, the particles are not only reduced in size, but dislocations and vacancies are created, thereby increasing the kinetics and capacity of the material. The interaction of the various particles that make up the hydrogen storage material are also of great importance, as this determines the interaction of the various compounds and either facilitates or hinders successful hydrogen sorption as will be shown.
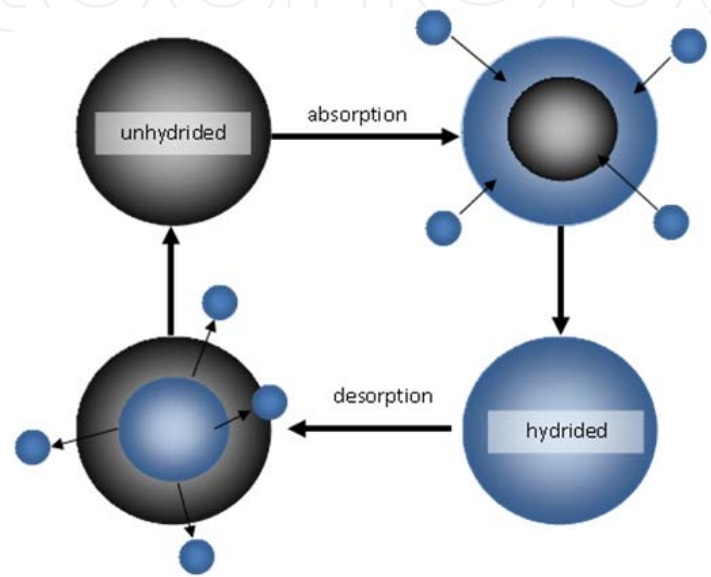

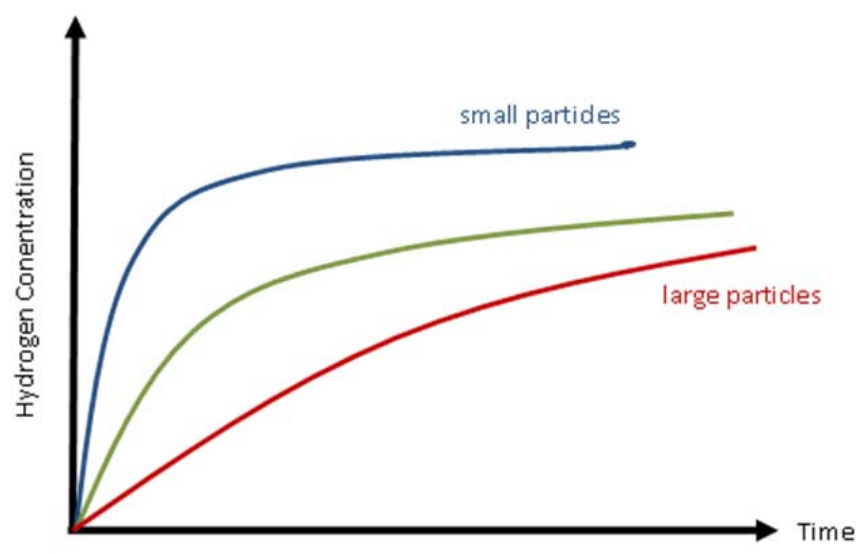**Figure 2.** Hydrogen storage mechanism in complex hydrides and the effect of particle size.

Figure 3. Particle size effects on hydrogen storage.

The complex hydrides that are developed are carefully investigated employing varying processing techniques, a deviation of the traditional means of producing complex hydrides. The nanostructure created with the varying techniques is carefully analyzed and correlated

with the material's hydrogen performance. Additionally, the hydrogen storage properties are significantly improved by using optimized quantities of nano sized additives.

2. Hydrogen sorption characteristics of polyaniline nanofibers

The conducting polymer nanostructures combine the advantages of organic conductors and low dimensional systems possessing interesting physicochemical properties (Macdiarmid & Epstein, 1989; Stejskal et. al., 1996; Stejskal & Gilbert, 2002; Trivedi, 1997) and useful applications (Fusalba et. al., 2001; Rossberg et. al., 1998; Virji et. al., 2006). Among the conducting polymers, polyaniline is considered important because of its extraordinary properties of electrical and optical behavior. It was recently reported that polyaniline could store as much as 6 to 8 weight percent of hydrogen (Cho et. al., 2007), which was later refuted. (Panella et al., 2005). Though many controversial results were reported in terms of hydrogen uptake (Cho et. al., 2007; Germin et. al., 2007; Jurczyk et. al., 2007; McKeown et. al., 2007) in polymer nanocomposites, there are still a number of parameters, tailor-made properties, surface morphologies and their correlation with hydrogen sorption behavior to be investigated before these materials can be commercially deployed for on-board hydrogen storage. Similarly, nanotubes (Dillon et. al., 1997; Nikitin et. al., 2008) or nanofibers (Hwang et. al., 2002) have attracted more interest because of their novel properties and wide potential for nanometer-scale engineering applications.

It is known that the nanofibrillar morphology significantly improves the performance of polyaniline in many conventional applications involving polymer interactions with its environment (Wang & Jing, 2008). This leads to faster and more responsive chemical sensors (Sadek et. al., 2005; Virji et. al., 2006), new organic/polyaniline nanocomposites (Athawale & Bhagwat, 2003) and ultra-fast non-volatile memory devices (Yang et. al., 2006). Nanofibers with diameters of tens of nanometers appear to be an intrinsic morphological unit that was found to naturally form in the early stage of chemical oxidative polymerization of aniline. In conventional polymerization, nanofibers are subject to secondary growth of irregularly shaped particles that form the final granular agglomerates. The key to producing pure nanofibers is to suppress secondary growth. Based on this, many methods (interfacial polymerization, rapidly mixed reactions, controlling pH and oxidizing agent) have been developed that can readily produce pure nanofibers with uniform growth, chemical composition and morphology (Ding & Wei, 2007; Rahy et. al., 2008). With this nanofiber morphology, dispensability and processbility of polyaniline are now greatly improved. On the other hand, the template synthesis method is an effective way to grow the nanotubes of various conducting polymers (Huczko, 2000). The preparation conditions and their effect on morphology, size, and electrical properties of nanofibers have been reported elsewhere (Zhang & Wang, 2006). Recently, a novel, simple, and scalable technique to control the formation of the nanofibers of polyaniline and its derivatives via porous membrane controlled polymerization (PMCP) was reported (Chiou et. al., 2008). Through appropriate synthesis conditions, nearly 100% nanofibers are formed with diameters tunable from 20nm to 250nm via the selection of pore diameter, monomer, counter ions, and polymerization conditions. The nanofiber lengths vary from sub-micrometer to several micrometers.

Conducting polyaniline nanofibers were synthesized using chemical templating method followed by electrospun process. These nanofibers have been compared with their standard bulk counterpart and found to be stable up to 150°C. Polyaniline nanofibers prepared by electrospun method reveal high hydrogen uptake of 10wt.% at around 100°C in the first absorption run. However, in the consecutive hydrogenation and dehydrogenation cycles, the hydrogen capacity diminishes. This is most likely due to hydrogen loading into the polymer matrix, chemisorption and saturation effects. A reversible hydrogen storage capacity of ~3-10 wt.% was also found in the new batch of electrospun nanofibers at different temperatures. The surface morphologies before and after hydrogen sorption of these PANI nanofibers encompass significant changes in the microstructure (nanofibrallar swelling effect) which clearly suggest effective hydrogen uptake and release.

Fourier Transform Infrared (FTIR) spectra of PANI-NF-CM and PANI-NF-ES prepared confirmed the formation of PANI in its emeraldine form. The major bonding environment remains unchanged for both structures (see Figure 4). The presence of two bands in the vicinity of $1500cm^{-1}$ and $1600cm^{-1}$ are assigned to the non-symmetric C6 ring stretching modes. The higher frequency vibration at $1600cm^{-1}$ is for the quinoid rings, while the lower frequency mode at $1500cm^{-1}$ depicts the presence of benzenoid ring units. Furthermore, the peaks at $1250cm^{-1}$ and at $800cm^{-1}$ are assigned to vibrations associated with the C-N stretching vibration of aromatic amine out of plane deformation of C-H of 1,4 disubstituted rings. The aromatic C-H bending in the plane ($1167cm^{-1}$) and out of plane ($831cm^{-1}$) for a 1,4 disubstituted aromatic ring indicates a linear structure.
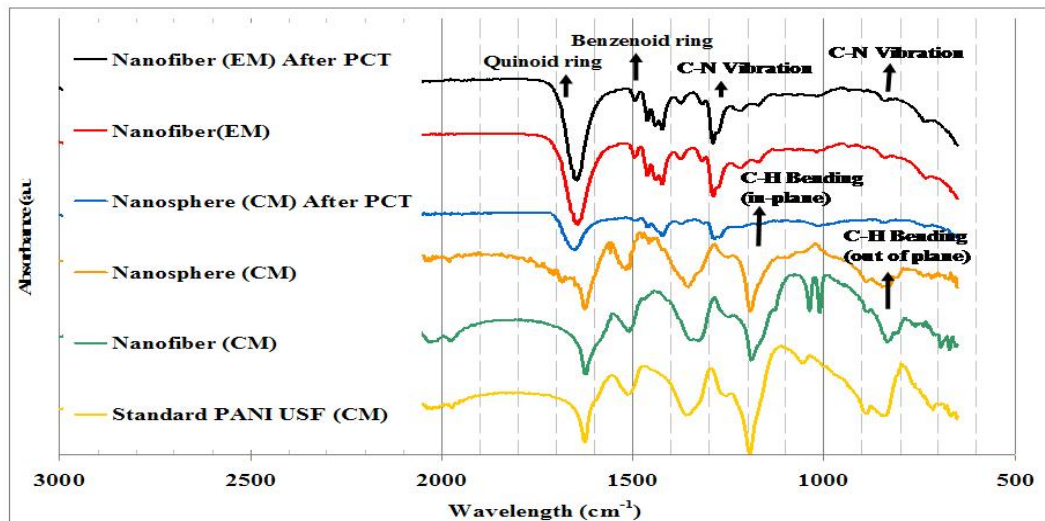

Figure 4. FTIR spectra of polyaniline nanofibers and nanospheres.

Figure 5(a) represents the scanning electron micrograph of PANI-NF-CM and Figure 5(b) shows the structure of the PANI-NF-ES sample. It is clear that the electrospun nanofibers exhibit a smoother surface as opposed to the rough surface of the chemically grown nanofibers. Figure 6 shows the cycle life kinetics of the electrospun PANI nanofibers. No hydrogen uptake was observed until the sample was heated to 100°C. The initial high capacity of 11wt.% is not fully observed when desorbing the hydrogen, as only 8wt.% is

released. This occurs in a two-step process characterized by a fast (physisorption) hydrogen release and a slower (chemisorption) hydrogen release step. The full capacity of hydrogen desorbed is then reabsorbed and with each consecutive cycle the amount of hydrogen dwindles until finally no more hydrogen is released of absorbed. This hydrogen behavior is due to hydrogen bonding with both unterminated bonds as well as with the surface of the nanofibers.
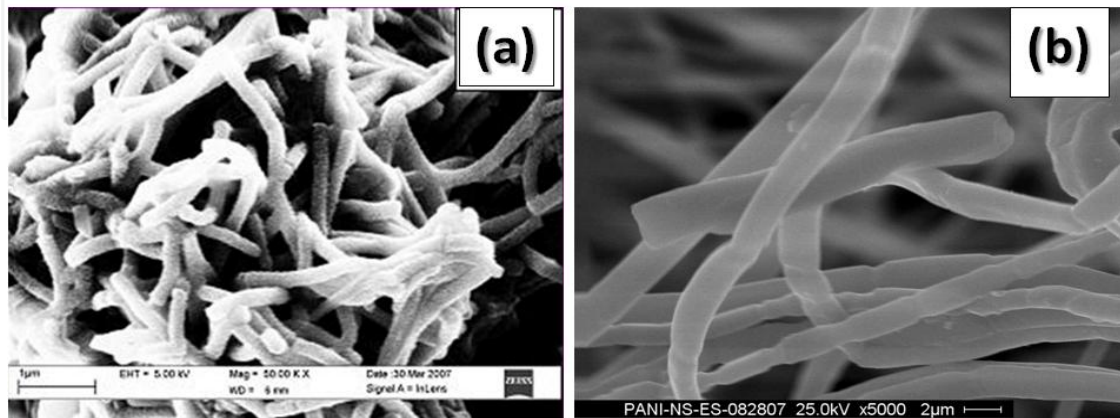

Figure 5. SEM micrographs of polyaniline nanofibers **(a)** chemically grown and **(b)** electrospun.

Pressure-Composition-Temperature (PCT) profiles of the PANI-NF-ES during hydrogen adsorption and desorption were plotted in Figure 7. Hydrogen storage capacity increases with increasing temperature from 50 to 125 °C in various cycles as shown Figure 7(a). At lower temperature of 50 °C, a hydrogen capacity of 3 wt.%, whereas at 100–125 °C, at least two fold increase of capacity (6–8 wt.%) was invariably obtained at various hydrogenation cycles. At the end of each adsorption PCT, desorption PCT experiments were performed by reducing the hydrogen pressure in steps of $\Delta P = 3$ bar, and are depicted in Figure 7(b). A hydrogen storage capacity of 2–8 wt.% was obtained at temperature range of 50–125 °C.
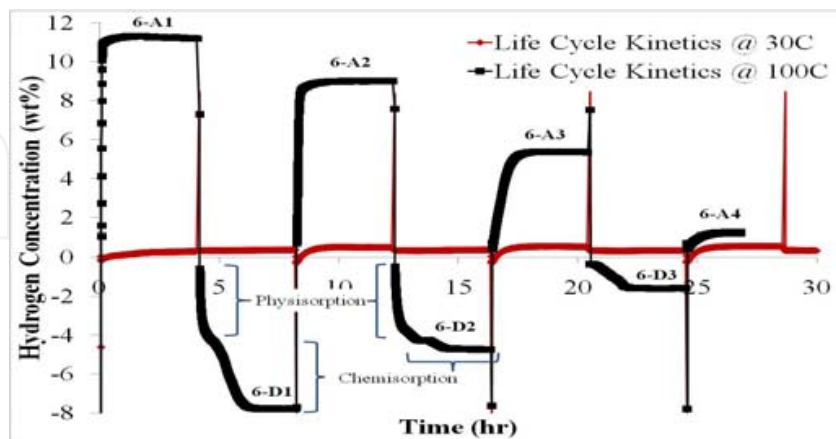

Figure 6. Hydrogen sorption kinetics in PANI-NF-ES.

Figure 8(a) represents the hydrogen absorption kinetic curves of the PANI-NF-ES sample after 55 previous sorption cycles at 30 °C. It can be seen that after approximately 2 h at 80 bar of H_2 pressure close to 5 wt.% of hydrogen is absorbed.

From the same figure, the hydrogen desorption was plotted after 66 cycles at 100 °C and reveals that the kinetics are rather rapid, with most of the hydrogen being released in less than 30 min for a total hydrogen release of close to 6 wt.%. Additionally, the absorption kinetics in the 64th cycle of hydrogen at 80 bar pressure with varying temperature is shown in Figure 8(b). Initially, the hydrogen is absorbed at 125 °C with saturation occurring after approximately 2 h (solid line). After 18 h, the temperature (dotted line) is reduced to 30 °C, whereupon another 3 wt.% of hydrogen is absorbed. This may be due to both chemisorption and physisorption phenomena occur in these materials and the mechanism is yet to be investigated.
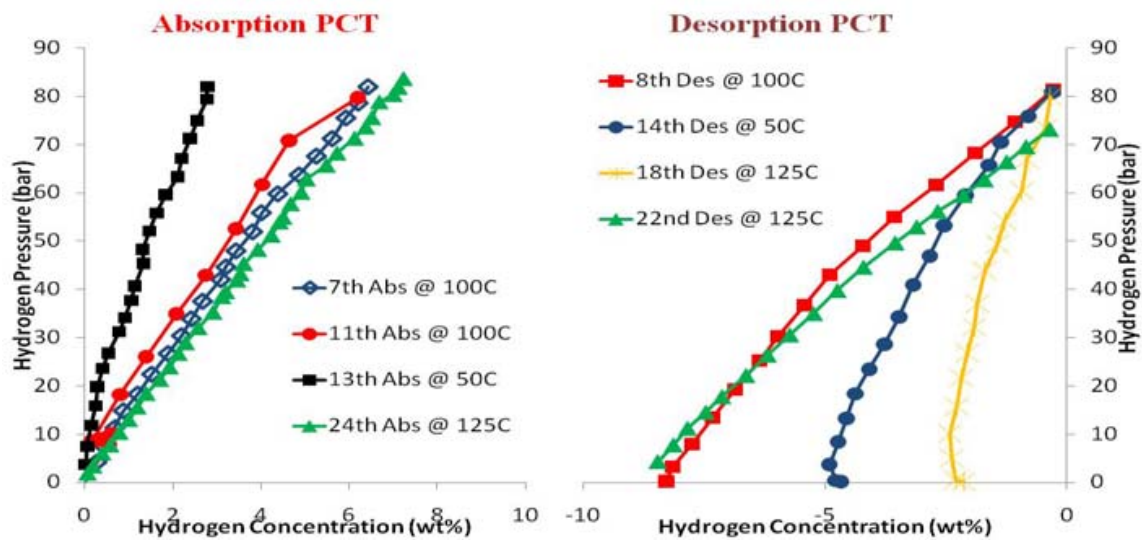

Figure 7. Hydrogen (a) adsorption and (b) desorption PCT curves for the PANI-NF-ES.
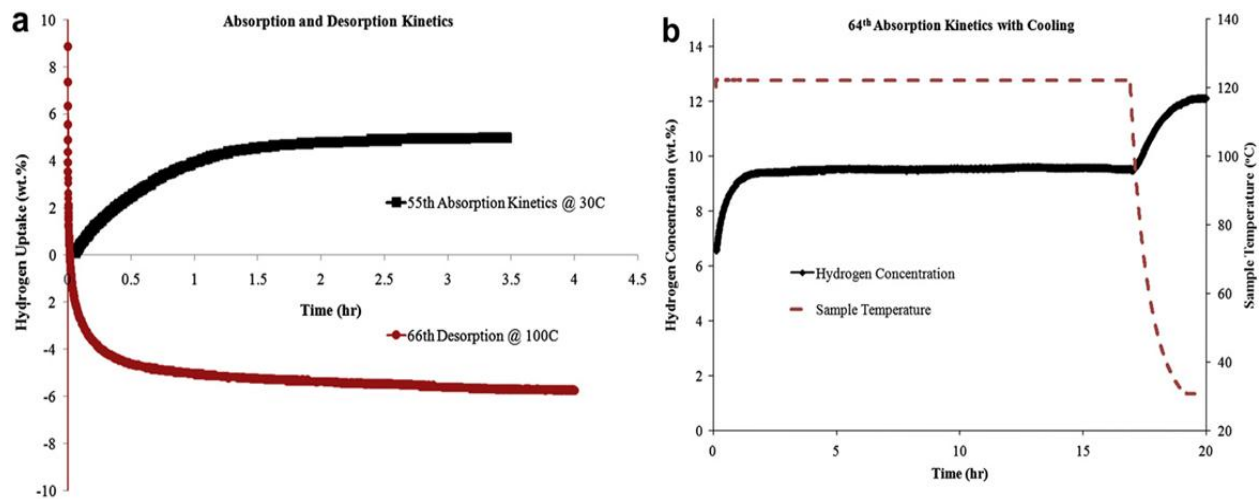

Figure 8. Hydrogen sorption kinetic curves of PANI-NF electrospun samples at different cycles.

The PANI-NF-CM, however, absorbed hydrogen at 30°C and did so reversibly with a capacity of approximately 3wt.%, as seen in Figure 9. Unlike the electrospun nanofibers, the hydrogen was absorbed and released in a one-step process with very rapid kinetics of less than 10min. This fast hydrogen sorption is most likely due to the higher surface area of the

chemically grown nanofibers as opposed to the electrospun nanofibers that exhibit a much smoother surface.

When looking at the microstructure of both types of polyaniline nanofibers, it is interesting to note that the nanofibers that were initially present, for the chemically grown samples have disappeared completely, as shown in Figure 10(a). BET surface area measurements, however, have shown that the surface area of the PANI-NF-CM has actually stayed constant, which is explained by the porous nature of the sample of hydrogen cycling. The hydrogen interacted with the PANI-NF-CM and created diffusion pathways for it to pass through the sample reversibly.
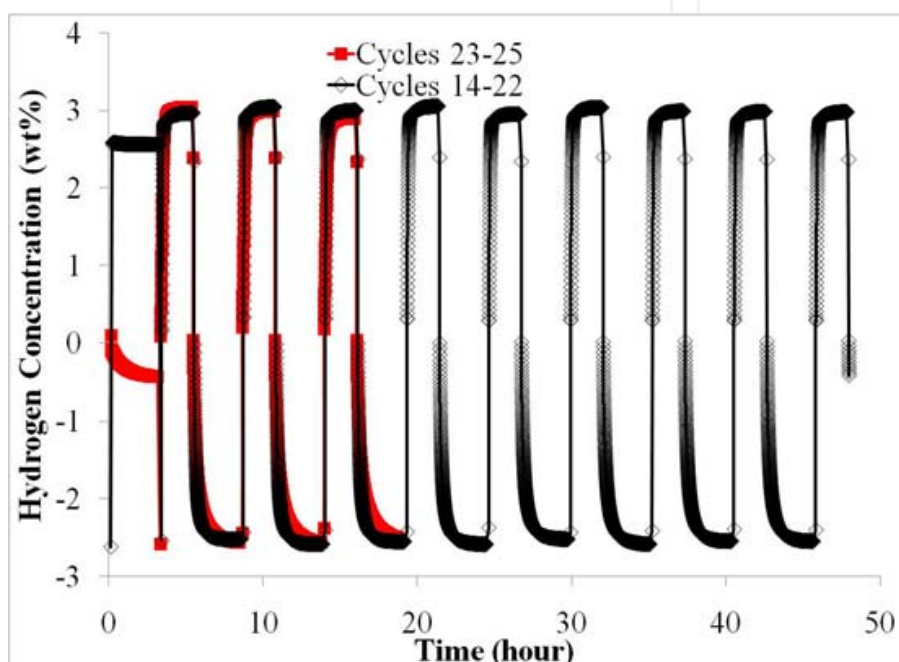

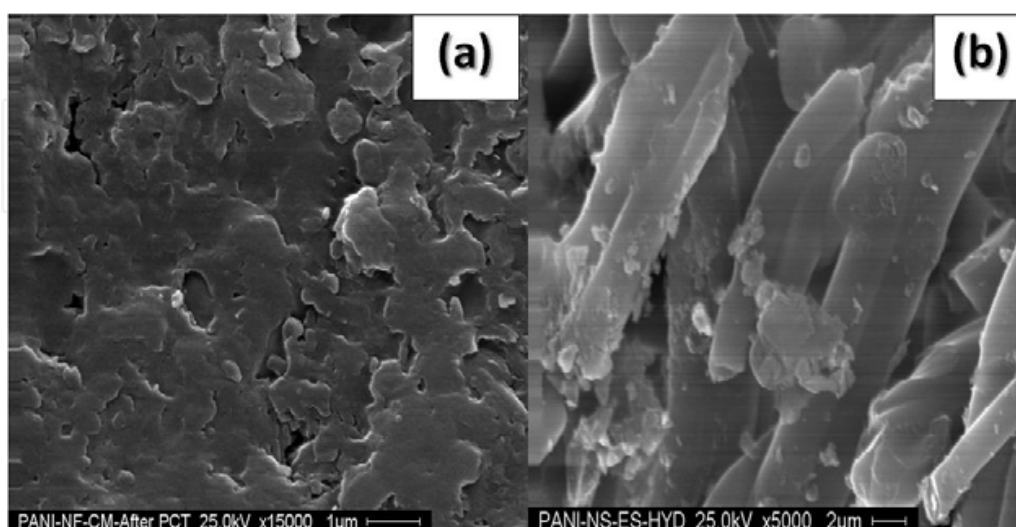**Figure 9.** Hydrogen sorption kinetics in PANI-NF-CM.

Figure 10. SEM micrographs of polyaniline nanofibers **(a)** chemically grown and **(b)** electrospun after hydrogen cycling measurements.

The microsturcture of the hydrogen cycled PANI-NF-ES, on the other hand, as shown in Figure 10(b), clearly show that the nanofibrallar structure is still intact, although the nanofibers show clear evidence of swelling and also of breaking apart. This further confirms the point that the hydrogen interacted more in a chemisorption manner with the sample, rather than physisorption.

3. Nanoscale complex multinary hydrides for reversible hydrogen storage

Advanced complex hydrides that are light weight, low cost and have high hydrogen density are essential for on-board vehicular storage (Grochala & Edwards, 2004; Schlapbach & Zuttel, 2001; Stefanakos et. al., 2007; US Department of Energy (DOE) Report 2003) Some of the complex hydrides with reversible capacities achieved are Alanates (Bogdanovic & Schwickardi, 1997; Jensen & Zidan, 2002; Srinivasan et. al., 2004), Alanes (Graetz et. al., 2005), Amides (Chen et. al., 2002; Hu & Ruckenstein, 2005) and Borohydrides (Au, 2006; Srinivasan et. al., 2008; Vajo et. al., 2005) magnesium based hydrides (Orimo et. al., 2005; Srinivasan et. al., 2006) and mixed complex hydrides (Jurczyk et. al., 2007) have been recently reported with improved hydrogen storage characteristics. The challenging tasks to design and develop the complex hydrides mandate an optimization and overcoming of kinetic and thermodynamic limitations (Fitchner, 2005; Zuttel, 2004). The enhancement of reaction kinetics at low temperatures and the requirement for high hydrogen storage capacity (> 6.5 wt.%) of complex hydrides could be made possible by either adopting destabilization strategies or catalytic doping. If nanostructured materials with high surface area are used as the catalytic dopants, they may offer several advantages for the physico-chemical reactions, such as surface interactions, adsorption in addition to bulk absorption, rapid kinetics, low temperature sorption, hydrogen atom dissociation and molecular diffusion via the surface catalyst.

The intrinsically large surface areas and unique adsorbing properties of nanophase catalysts can assist the dissociation of gaseous hydrogen and the small volume of individual nanoparticles can produce short diffusion paths to the materials' interiors. The use of nanosized dopants enables a higher dispersion of the catalytically active species (Joo et. al., 2001) and thus facilitates higher mass transfer reactions. Recently, it is claimed that an enhancement of reaction kinetics has been demonstrated with CNT catalyzed $NaAlH_4$ as represented in Figure 14a and 14b (Dehouche et. al., 2005). It was speculated that the repeated interactions of CNT with $NaAlH_4$ during mechanical milling causes an insertion of nanotube bundles (~100-200 nm) in $NaAlH_4$ matrix and accompanying deformation as shown in Figure 14c (Pukazhselvan et, al., 2005).

In addition, the structure of carbon plays an important role on the hydrogenation and dehydrogenation behavior of $NaAlH_4$. Improvement of reaction rate and hydrogen storage capacity has also been reported for the Alanates doped with Ti-nanoparticles (Bogdanovic et. al., 2003). Apparently, the use of nanosized doping agents enables one to achieve a higher dispersion of the catalytically active Ti species than their bulk counterparts. Though the catalytic enhancement of decomposition of sodium aluminum hydride leads to fast sorption

kinetics at moderate temperatures, its usable hydrogen storage capacity is rather limited (~5.6 wt%). Lithium borohydride (LiBH$_4$) on the other hand, possesses theoretical hydrogen content of ~18.3 wt%, exhibiting potential promise for on-board applications. However, hydrogen decomposition from LiBH$_4$ starts at an elevated temperature of 380 °C and also shows little or no reversible hydrogenation behavior. It has been reported that catalytically doping SiO$_2$ lowers the temperature of hydrogen evolution to 300 °C (Zuttel et. al., 2003). In addition to improving the kinetics of LiBH$_4$, tailoring the thermodynamic property is of vital importance for developing an ultimate "holy grail" material for hydrogen storage.

In this direction, the hydrogenation/dehydrogenation enthalpy has been reduced by 25 kJ/mol of H$_2$ for the (LiBH4+½ MgH$_2$) system (Vajo et. al., 2005). Magnesium hydride destabilizes the LiBH$_4$ structure and forms an intermediate MgB$_2$ phase (Barkhordarian et. al., 2007; Cho et. al., 2006) during the hydrogen charging and discharging reactions. In a very recent study on the LiBH$_4$/MgH$_2$ system, it was demonstrated that the hydrogenation and dehydrogenation of LiBH$_4$ occurs via the Li-Mg alloy phase (Yu et. al., 2006) and not through MgB$_2$ formation. It is generally known that pristine MgH$_2$ theoretically can store content of ~7.6 wt.% hydrogen (Zaluska et. al., 2001). However, so far, magnesium hydride based materials have limited practical applications because both hydrogenation and dehydrogenation reactions are very slow and hence relatively high temperatures are required (Schlapbach & Zuttel, 2001). Magnesium hydride forms ternary and quaternary hydride structures by reacting with various transition metals (Fe, Co, Ni, etc) and thus improved kinetics (Jeon et. al., 2007). Moreover, the nanoscale version of these transition metal particles offers an additional hydrogen sorption mechanism via its active surface sites (Jeon et. al., 2007; Zaluska et. al., 2001). In a similar way, the synergistic approach of doping nanoparticles of Fe and Ti with a few mol% of CNT on the sorption behavior of MgH$_2$ has recently been investigated (Yao et. al., 2006). The addition of Carbon Nanotubes (CNT) significantly promotes hydrogen diffusion in the host metal lattice of MgH$_2$ due to the short pathway length and creation of fast diffusion channels (Wu et. al., 2006).

The dramatic enhancement of kinetics of MgH$_2$ has also been explored through reaction with small amounts of LiBH$_4$ (Johnson et. al., 2005). Though the MgH$_2$ ad-mixing increases the equilibrium plateau pressure of LiNH$_2$ (Luo, 2004) or LiBH$_4$ (Rivera et. al., 2006; Vajo et. al., 2005), catalytic doping of these complex hydrides had not been investigated. It is generally believed that the role of the nanocatalyst on either NaAlH$_4$ or MgH$_2$ is to stabilize the structure and facilitate a reversible hydrogen storage behavior. However, the actual mechanism by which transition metal nanoparticles enhance the dehydrogenation kinetics of complex hydrides is not yet understood very well. Thus, it is desirable to investigate the effects of catalysts, defects, grain boundaries, interface boundaries and impurity atoms on the surface. Based on an extensive literature search, we found no reports on the synergistic effects of transition metal nanoparticles on the complex composite hydrides such as LiBH$_4$/MgH$_2$, LiNH$_2$/LiH/MgH$_2$ or LiBH$_4$/LiNH$_2$/MgH$_2$ etc.

The present work addresses the grand challenge of hydrogen storage by mechano-chemically milling LiBH$_4$ and LiNH$_2$ with MgH$_2$ to produce a new complex quaternary Li-Mg-B-N-H structure. This Li-Mg-B-N-H structure possesses storage capacity of more than

10 wt.% at around 150 °C. The parent compounds, $LiBH_4$ and $LiNH_2$, were purchased from Sigma Aldrich with a purity of at least 95%, while MgH_2 was obtained from Alfa Aesar with a purity of 98%. All materials were kept in an inert atmosphere in a glove box and used without further purification. The investigated samples were created in 4g batches with a constant molar ratio of $2LiNH_2:LiBH_4:MgH_2$, while taking into account the purity of the parent compounds, by employing high energy ball milling (Fritsch Pulverisette 6) for 5 hours at 300rpm with intermittent hydrogen/argon (5%/95%) purges for 20 minutes before milling and after 2 and 4 hours. This was done to ensure that as little hydrogen as possible was released during the milling process and to reduce the agglomeration of the hydride that occurs when pure hydrogen is used as compared to the hydrogen/argon mixture. The MgH_2 was either added as received or was added as a so-called nano MgH_2. The nano MgH_2 ($nMgH_2$) was created by ball milling the commercial MgH_2 ($cMgH_2$) for 12 hours with intermittent hydrogen/argon purges every 2 hours. This ensured the reduction of particle size as well as the decrease in hydrogen release temperature, as previously reported. The two main processing schemes that were used are shown in Figure 11.

The first processing scheme was to add all parent compounds and mill for 5 or 10 hours using either commercial or nano MgH_2. This is the scheme that is generally used in reported literature and the materials serve as a kind of reference material. The second processing scheme was to first create the quaternary structure LiBNH by milling $LiBH_4$ with $2LiNH_2$ for five hours and then adding either commercial or nano MgH_2, after which the quaternary and the MgH_2 were milled for an additional 5 hours. All milling was carried out in an inert atmosphere and the samples were purged with the hydrogen/argon mixture every 2 hours. In total, five different samples were created. The samples are referred to in this paper according to the naming convention shown in the bold boxes of Figure 11.
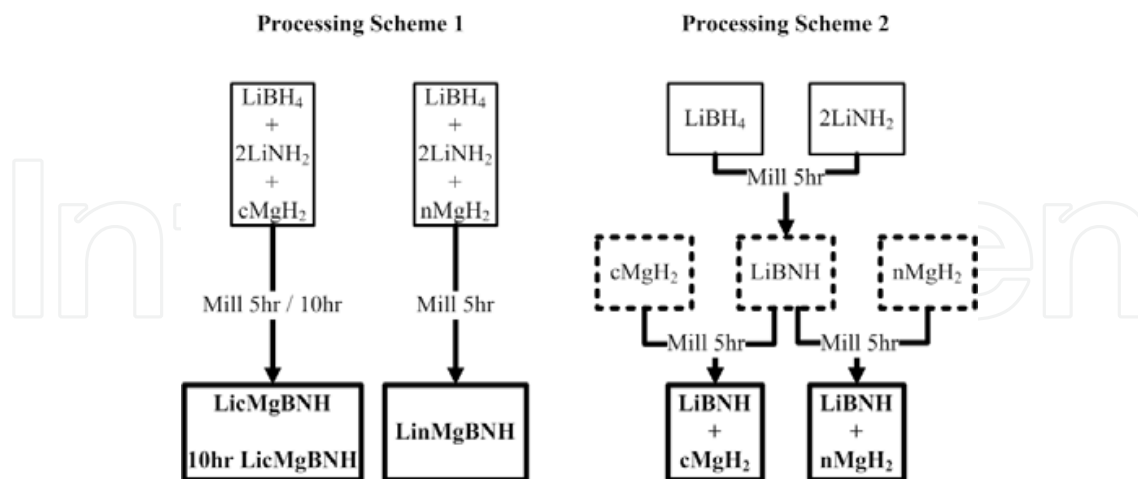

Figure 11. Processing schemes of synthesizing complex hydrides LiBH4/2LiNH2/nanoMgH2 via reactive gas milling.

X-Ray Diffraction. Figure 12 shows the XRD pattern comparing the five differently processed complex hydrides. The parent compounds, $LiBH_4$, $LiNH_2$, as well as both commercial and nano MgH_2 are in the lower half of the figure as a reference. Neither $LiBH_4$ nor $LiNH_2$ peaks

are observed in any of the five samples. This confirms that these two materials are fully consumed during the milling process and actually form a new quaternary structure, referred to as LiBNH. The addition of commercial MgH$_2$ does not cause the formation of a new complex structure, but instead indicates that the quaternary structure is preserved, while the MgH$_2$ simply intermixes with the material. When the nano MgH$_2$ is added to LiBH$_4$ and LiNH$_2$ or to the quaternary LiBNH, the MgH$_2$ peaks are barely picked up by the XRD. This indicates that the small size of the MgH$_2$ causes the material to intermix and fill voids of the quaternary structure, which results in a nanocrystalline particle distribution, while still preserving the quaternary structure formed by the LiNH$_2$ and LiBH$_4$. All samples are a physical, rather than a chemical, mixture of the quaternary structure LiBNH with MgH$_2$.

Thermal programmed desorption. Upon producing the complex hydrides, each sample was characterized for its thermal desorption characteristics using TPD with a heating rate of 1, 5, 10, and 15°C/min. As compared to the quaternary structure, the multinary structure containing MgH$_2$ showed a 3-step hydrogen release mechanism, as is shown in Figure 13. Our TPD analysis of LicMgBNH sample confirms the previously reported data (Yang et al.), but also shows that the processing condition of the material does have an effect on the thermal decomposition characteristics. The first hydrogen release peaks between 157.7^{o}C for 10hr LicMgBNH and 165.2^{o}C for LinMgBNH, which is a relatively small difference in temperature. When investigating the second, or main, peak of the various samples, it is interesting to note that the temperature range for main hydrogen release varies from 287°C for the 10hr LicMgBNH to 306.6^{o}C for LinMgBNH. MgH$_2$ interacts with the quaternary structure and destabilizes it, thereby releasing hydrogen. In the case of the LinMgBNH and LicMgBNH samples, it takes the entire milling duration (5hr) to form the quaternary phase, thereby giving the MgH$_2$ little time to allow for the release of hydrogen during milling. In the case of 10hr LicMgBNH, the MgH$_2$ has 5hr of milling duration (after the formation of the quaternary) to destabilize the material and allow for hydrogen release.

Finally, in the case of LiBNH+cMgH$_2$, the MgH$_2$ has to first be reduced in size to allow for the destabilization and the resultant hydrogen release. LiBNH+nMgH$_2$, however, releases hydrogen during the milling process, as the smaller size of nano MgH$_2$ allows for immediate destabilization of the already present quaternary. Either prolonged milling duration or reduction in particle size will lead to release of hydrogen in the milling process

Activation energy. The activation energy of each sample was experimentally determined using Kissinger's method, based on TPD data (Figure 13) taken at 1, 5, 10, 15°C/min for the two peaks and correlated to the hydrogen peak release temperature as described by:

$$\frac{d\left(\ln\frac{\beta}{T_m^2}\right)}{d\left(\frac{1}{T_m}\right)} = -\frac{E}{R}$$

where β is the heating rate of the sample in K/min, T_m is the peak temperature in K, E is the activation energy of the hydrogen release, and R is the gas constant. When investigating the first peak, around 160°C, it is interesting to note that the 10hr LicMgBNH sample has the

lowest activation energy (109.8 kJ/mole) at 157.7°C as seen in Figure 14. Although all samples exhibit comparable decomposition temperatures, their activation energies vary by ~20 kJ/mole.
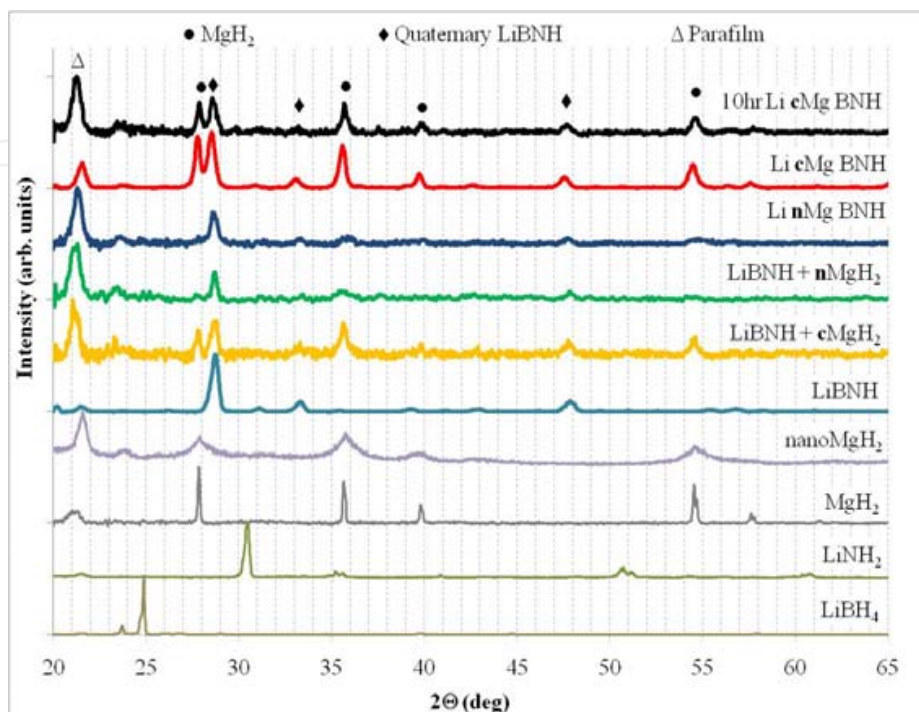

Figure 12. XRD Profile of the five differently processed materials as well as the parent compounds, LiBH₄, LiNH₂, MgH₂ and nano MgH₂.
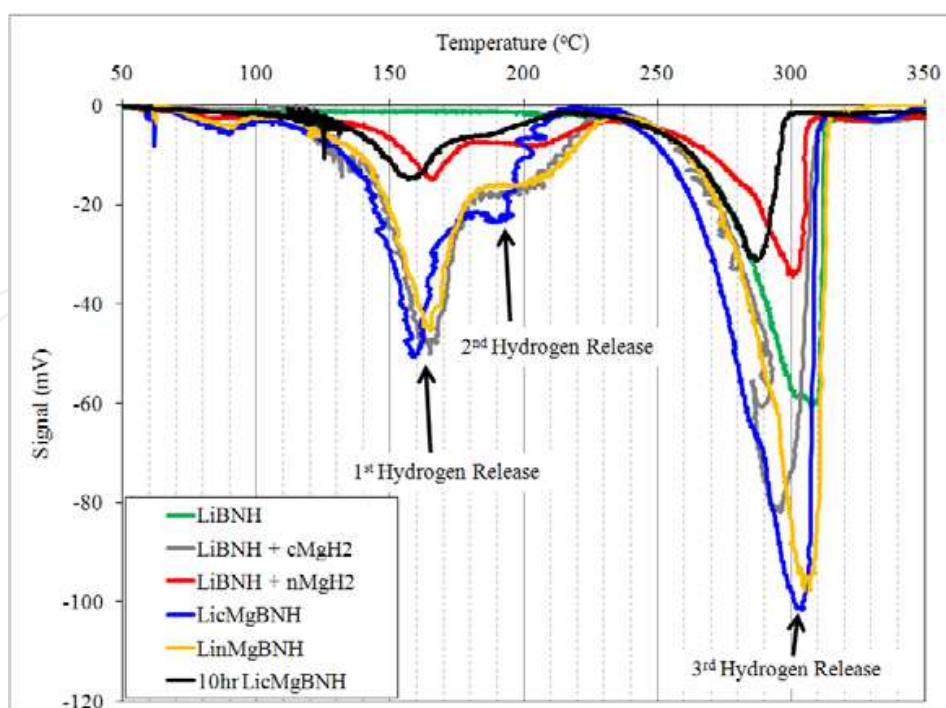

Figure 13. TPD comparison of investigated processing variations showing the two main hydrogen release regions around 160°C and 300°C.
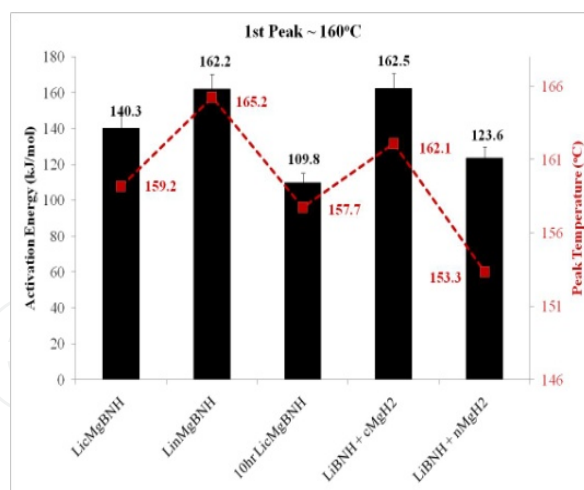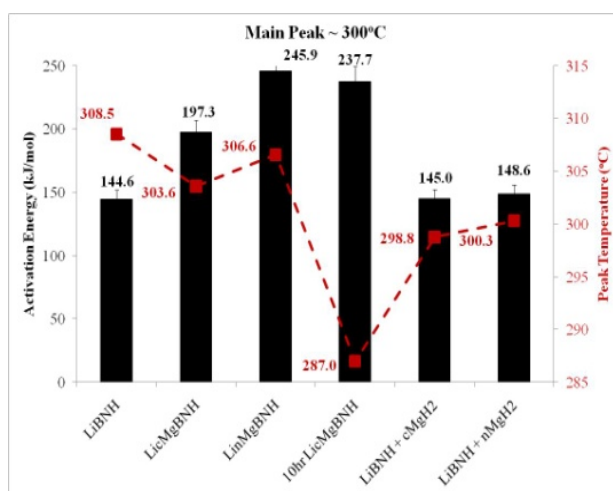
Figure 14.

Figure 15. Activation energy, as calculated from the TPD data using Kissinger's method, compared with the first and main peaks of hydrogen release temperature.

A plausible reason is that the reaction pathways of ad-mixing MgH_2 either in the first place (10hr LicMgBNH) or after the quaternary formation (e.g. LiBNH+nMgH_2) proceeds with fine distribution of nanocrystalline MgH_2 in the host matrix of multinary hydrides. It has been recently claimed that the nanocrystallization of MgH_2 has significant impact on lowering the enthalpy of formation and enhancement of the reaction kinetics. The high temperature main hydrogen release peak (300°C) for all the processed materials and the reference LiBNH quaternary hydride are shown in Figure 6. While comparing the activation energies and decomposition temperatures of all the samples, it can be clearly inferred that the quaternary hydrides LiBNH combined with either commercial (LiBNH+cMgH_2) or nanocrystalline MgH_2 (LiBNH+nMgH_2) milled for 5 hours show lower values, e.g. 145-148 kJ/mole at ~300°C. Simply based on this data, it is difficult to justify from both Figures 15 and 6, which sample possesses an optimum hydrogen release characteristic at these two main decompositions. However, it is undoubtedly clear that both the steps occur at two different temperature regimes, namely 160 and 300°C, at which either surface adsorbed or bulk absorbed hydrogen is released.

At the low temperature hydrogen release step, the nano MgH$_2$ acts as a facilitator in speeding up the reaction; hence both the 10hr LicMgBNH and LiBNH+nMgH$_2$ materials demonstrate lower activation energies (Figure 14). On the other hand, in the high temperature hydrogen release step (Figure 15), the temperature of 300°C acts as a driving force to release hydrogen from the bulk structures of both LicMgBNH and LinMgBNH milled only for 5 hours. Hence, these materials exhibit lower activation energies which are comparable to pristine LiBNH. Based on the detailed analysis, we draw the conclusion that an additional 5 hours of ball milling, either of the all-in-one hydride (10hr LicMgBNH) or the quaternary/nanocrystalline hydride mixture (LiBNH+nMgH$_2$), will alter the decomposition characteristics, especially the activation energy which is vital for hydrogen storage.

Pressure-composition-isotherms. Figure 16 represents the PC isotherms of the multinary complex hydrides created with different processing conditions. The PCT studies of the multinary samples are carried out under the following conditions: temperature, T=150-175°C; pressure difference between aliquots, ΔP=3bars (0.3 MPa); absorption pressure limit, P$_a$=80bars (8 MPa); desorption pressure limit, P$_d$=0bar (0 MPa); and reservoir volume, V$_r$=160cm^3. Since all these samples are in hydride phases, the dehydrogenation experiment was followed by the rehydrogenation for at least 10 hours.

The PCT characteristics and their observations are given with respect to the sample processing conditions as follows.

LicMgBNH and LinMgBNH: The multinary complex hydrides processed with either commercial or nanocrystalline MgH$_2$ and milled all-in-one for 5 hours reveal reproducible hydrogen capacity of 3 to 4wt.%. It is noteworthy to mention that LinMgBNH possesses at least 1wt.% higher capacity and 25°C reduction in temperature as compared to the LicMgBNH counterpart, as also seen from the initial ramping kinetic profiles in Figure 7b. This could be achieved because of the uniform distribution of fine MgH$_2$ nanoparticles which likely act as hydrogen diffusion enhancement sites, increasing the amount of hydrogen released. Yet another difference between these two processed materials is the tailoring of the plateau pressure (hydrogen/hydride equilibrium region), which is crucial for a hydrogen storage system to be viable for mobile applications. The LinMgBNH material exhibits reduction in the absorption plateau pressure by 20 bars (2 MPa) in contrast to the LicMgBNH due to nanoparticulate formation.

LiBNH+cMgH$_2$ and LiBNH+nMgH$_2$:A greater reversible hydrogen storage capacity of 5.3-5.8wt.% was found at temperatures of 150°C to 175°C for the quaternary hydrides LiBNH either milled with commercial or nano MgH$_2$ for 5 hours. The nano MgH$_2$ loaded LiBNH outperformed its commercial counterpart with a higher hydrogen capacity of 5.8wt.%. at 150°C as compared to 175°C (refer to Figure 16b). Figure 16a shows that there are plateau pressure regions, which are not as clearly defined as the LicMgBNH and LinMgBNH samples. Moreover, the sorption plateau of these samples resembles greatly the pristine LiBNH (not shown here), which is the precursor material for the multinary hydride formation. Overall, it is unambiguously claimed that LiBNH admixed either with

commercial or nano MgH_2 and milled for 5 hours, exhibits a high reversible hydrogen storage capacity of ~6wt.% at temperatures less than 175°C.
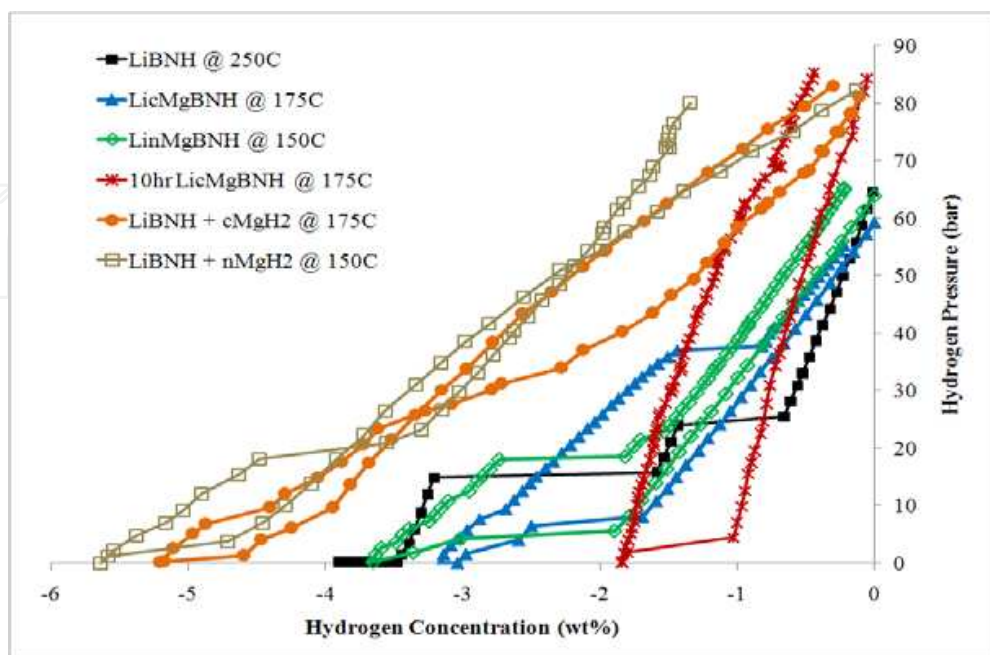

Figure 16. Comparison of the hydrogen sorption characteristics of the various processing conditions at the lowest hydrogen release temperature.

10hr LicMgBNH: The extended milling duration of 10 hours for the three component systems, $2LiNH_2+cMgH_2+LiBH_4$ show poor hydrogen performance as depicted in Figure16a. A low hydrogen desorption capacity of 2wt.% at a plateau pressure of less than 5bars (0.5 MPa) with little or no reversibility is obtained in this material. The crystallite agglomeration during the prolonged milling is expected to be the limiting factor for the absence of plateau pressure and overall storage capacity. Though this sample exhibits a lower activation energy (~109 kJ/mole) in the first hydrogen release (see Figure 14), the effective hydrogenation needs systematic optimization strategies which are currently under investigation.

Crystallite size effects on hydrogen release characteristics. In order to better understand the hydrogen performance of the differently processed materials, the hydrogen capacity was correlated with the crystallite sizes of the quaternary phase, LiBNH, and the MgH_2. The crystallite sizes were calculated from the XRD data (Figure 12) of each material using Scherrer's method. The initial crystallite sizes of $LiNH_2$, $LiBH_4$, MgH_2, nano MgH_2 and LiBNH were determined to be 138nm, 152nm, 212nm, 27nm, and 60nm, respectively. As seen from Figure 16b, the nano size MgH_2 has a definite effect on the initial hydrogen release temperature. Both samples synthesized with nano MgH_2 release hydrogen at 150°C as compared to 175°C for all the other samples, which were synthesized with its commercial counterpart. The MgH_2 crystallite size for the nano MgH_2 samples are both approximately 10nm, whereas the crystallite size of the commercial MgH_2 samples vary from 35nm to 75nm, as seen in Figure 17. It is important to note that the crystallite size of both MgH_2 and LiBNH are largest for the 10hr LicMgBNH sample, which explains the poor hydrogen

performance. This is because of the well known fact that larger particles, and therefore a smaller surface area, can limit hydrogen performance (less than 2wt.% capacity) due to diffusion inhibition and passivation effects.

A milling duration of more than 5 hours is in fact counterproductive and allows for the crystallite size to increase, as both the LiBNH and MgH$_2$ agglomerate. When looking at the correlation between crystallite size and hydrogen concentration, as shown in Figure 17, it becomes evident that the size of the LiBNH crystallites plays an important role on the amount of hydrogen released.
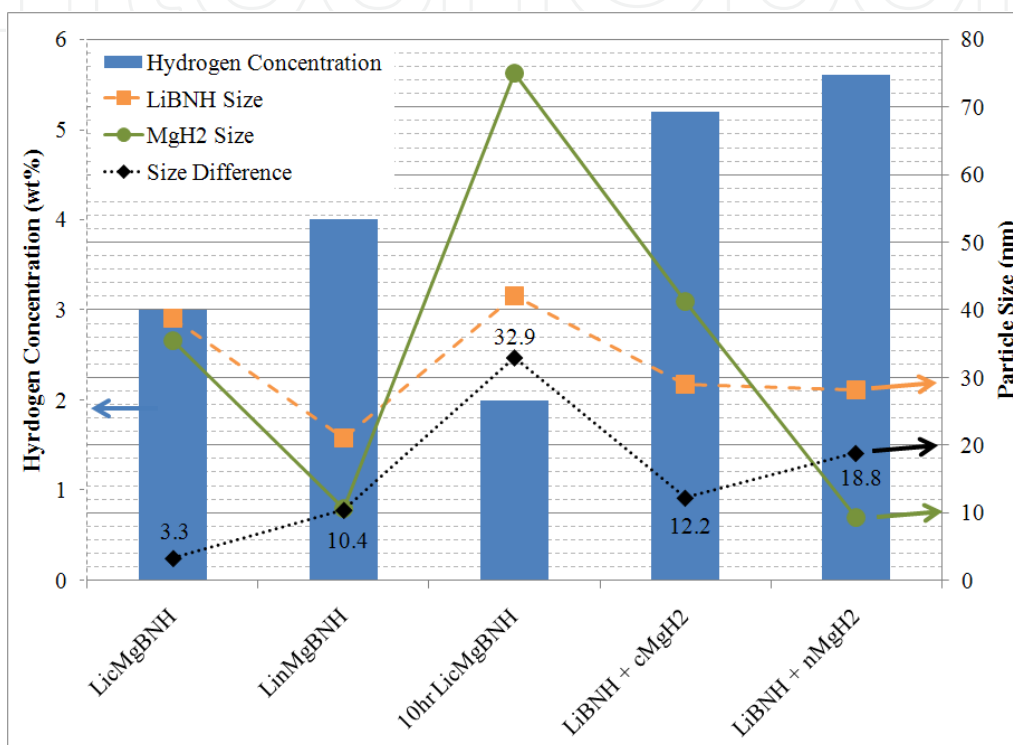

Figure 17. Comparison of hydrogen concentration and crystallite size of the quaternary LiBNH and MgH$_2$ phases after milling.

If the LiBNH crystallites have a size of approximately 28nm and the MgH$_2$ crystallites are approximately within 15nm (13nm to 43nm) of this size, the highest possible hydrogen release is achieved (5.5wt.%). When the MgH$_2$ and LiBNH crystallites are either too similar in size, as in the case for the LicMgBNH sample (3.3nm difference), or if they are too different in size, as in the case for the 10hr LicMgBNH sample (32.9nm difference), the amount of hydrogen released by the sample is reduced. Overall, the new multinary complex hydrides show potential promise on the reversible hydrogen storage characteristics as elucidated in Figure 18. The cyclic kinetics of Li-nMg-B-N-H reveals a reversible hydrogen storage capacity of 6-8wt.% with fast sorption kinetics around 200-250°C which matches or exceeds with the set-forth DOE technical targets. Thus a reversible hydrogen storage capacity of 5-7 wt.% was reproducibly obtained for these materials. With respect to the mass spec analyses, note that the scans did not reveal any evidence for potential parent (or daughter) species (ions); namely, NH$_3$, BH$_3$, BH$_2$NH$_2$, N$_2$H$_4$.

Destabilization of LiBH$_4$/LiNH$_2$/MgH$_2$ with Nano Sized Additives. Based on the previous experimental work on the optimization of the processing conditions as well as some previous insight into the role of nano sized additives on the quaternary LiBNH structure, it was decided to systematically investigate the effect of various nano sized additives on the multinary structure LiBNH + nMgH$_2$, as described in the previous section.
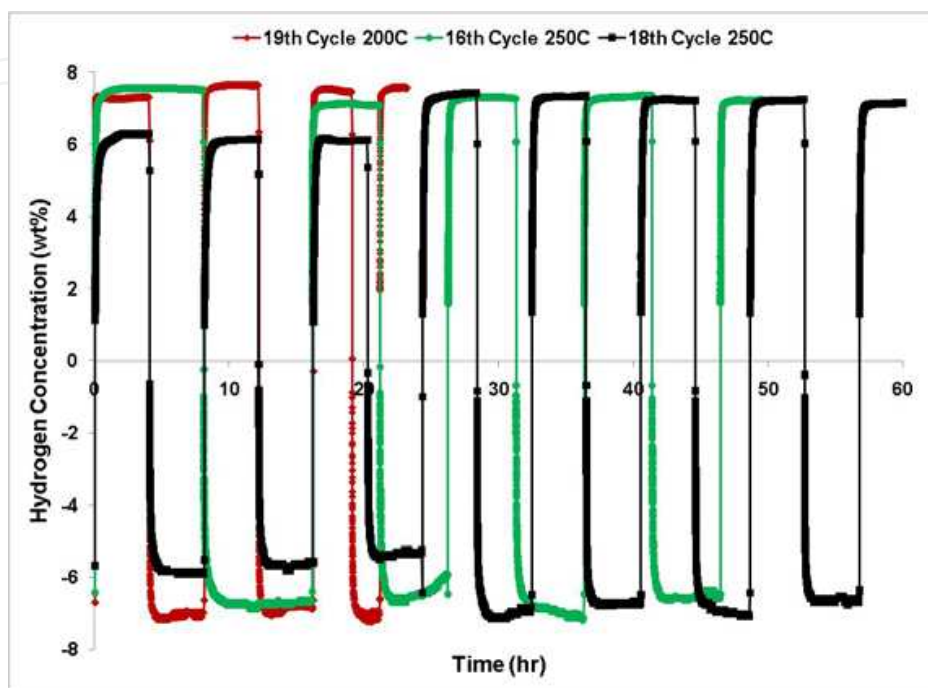

Figure 18. Dehydrogenation and reversible rehydrogenation cyclic kinetics in Li-nMg-B-N-H materials

TPD was used to obtain information about changes in the parent material's hydrogen characteristics. Specifically, the temperature of hydrogen release as well as some general information about the kinetics of hydrogen release can be ascertained from this type of measurement. The peak temperature indicates the optimal hydrogen release temperature, whereas the width of the peak can be used to get insight into the rate at which hydrogen is released, at least qualitatively. A wide peak indicates a low rate of hydrogen release, whereas a narrow and sharp peak indicates rapid hydrogen release. Figure 19 demonstrates the lower temperature release of hydrogen by nanoadditve doping when compared to the pristine complex hydride. As previously described, the parent compound, LiBNH + nMgH$_2$, exhibits a three-step hydrogen release. While the TPD measurements are used for quick-screening the effect of the additives on the hydrogen performance of the material, it can be seen that each additive material either affects the rate of hydrogen release, as depicted by a sharp and narrow peak (especially iron) or significantly lowers the temperature required for hydrogen release.

Since the TPD measurements only give an indication of the hydrogen sorption results, ramping kinetic measurements, where approximately 0.1g of sample are loaded into the PCT and then ramped at a rate of 1°C/min, were performed on all samples. Figure 20 shows the more detailed hydrogen performance of the standard sample, LiBNH+nMgH$_2$ without any additives, as well as with 2mol% of the aforementioned additives.
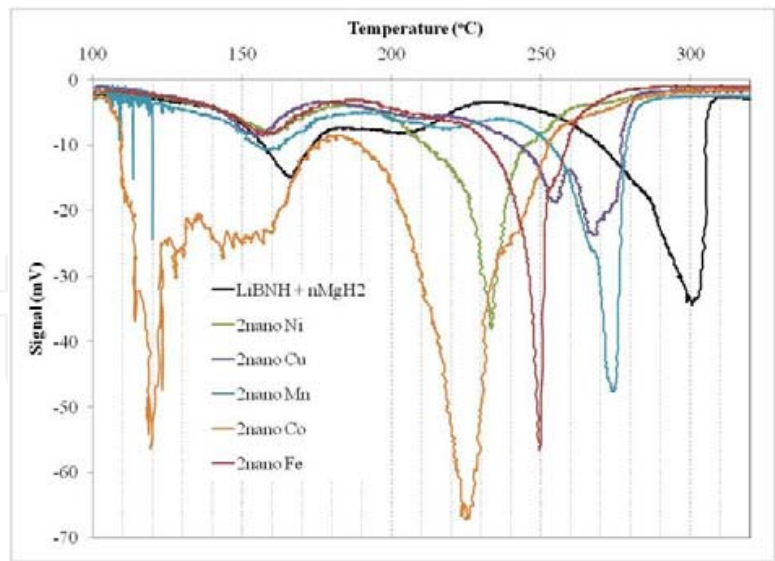
Figure 19. TPD comparison of LiBNH+nMgH₂ without additive and with 2mol% Ni, Cu, Mn, Co and Fe at a constant ramping rate of 1∘C/min.
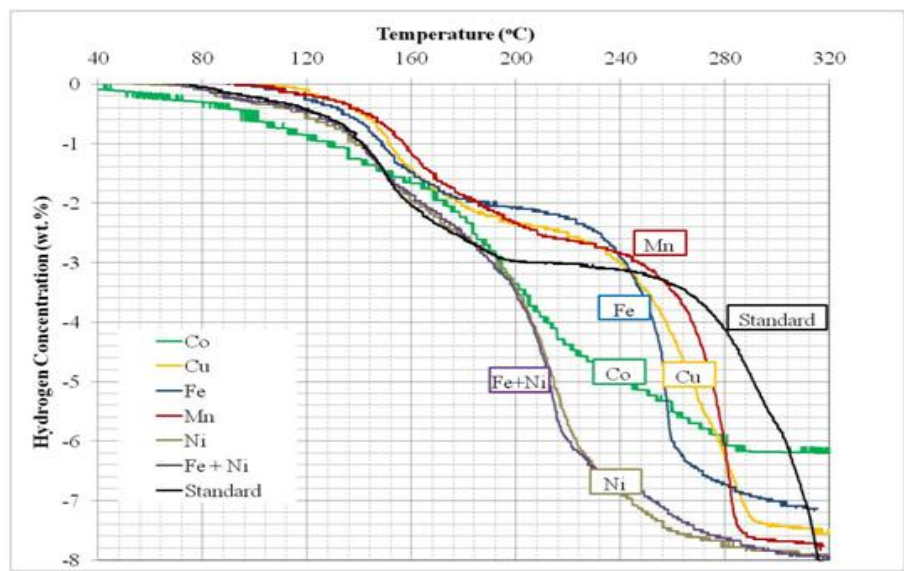

Figure 20. Ramping kinetics measurements of LiBNH+nMgH2 without and with 2mol% nano Mn, Fe, Co, Cu, Ni and Fe+Ni.

It becomes clear that while cobalt seemed promising from the TPD data, it in fact has such slow kinetics, that cobalt is no longer of interest as an additive. The kinetics measurement do confirm the TPD data in that manganese and iron have the fastest kinetics, as indicated by the slope of the desorption curves. Furthermore, the significant reduction in hydrogen release temperature of nickel is confirmed. Figure 21 shows a comparison of the hydrogen release rate and hydrogen release temperature of the standard sample without and with 2mol% of nano sized additives. Since the nano sized nickel showed the lowest hydrogen release temperature of just under 200∘C and nano sized iron showed the highest release rate (0.2wt.%/min) at a comparatively low temperature of 245∘C, these two additives were chosen to be optimized in terms of their concentration.
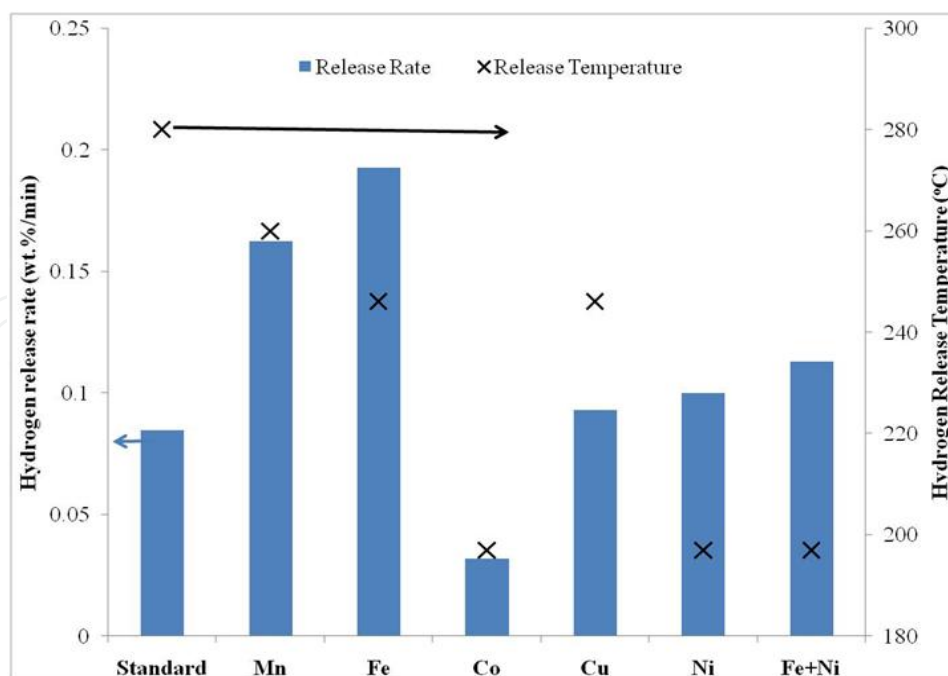
Figure 21. Comparison of hydrogen release temperature and hydrogen release rate of the standard
LiBNH+nMgH$_2$ and LiBNH+MgH$_2$ with 2mol% of various nano additives.

Material	Capacity	Reversibility	Temperature	Comments
PANI Bulk	0.4 wt%	Small	125°C	
PANI NS-CM	6 wt%	Decreases to 0.5 wt%	30°C	Slow kinetics (hours)
PANI NF-CM	3 wt%	Reversible	30°C	Fast Kinetics (<10min)
PANI NF-ES	10wt%	Reversible decreases with cycle kinetics	100°C (kinetic) 125°C (PCT)	Kinetics combination of physisorption and chemisorption

Table 1. Polyaniline Nanostructures and their hydrogen storage characteristics.

Material	Capacity	Reversibility	Temperature	Activation Energy
LicMgBNH	3.2 wt%	Reversible	175°C	140.3 kJ/mol
LinMgBNH	3.8 wt%	Reversible	150°C	162.2 kJ/mol
LicMgBNH 10hr	1.9 wt%	Reversible	175°C	109.8 kJ/mol
LiBNH + cMgH$_2$	5.2 wt%	Reversible	175°C	162.5 kJ/mol
LiBNH + nMgH$_2$	5.6 wt%	Reversible	150°C	123.6 kJ/mol

Table 2. Hydrogen storage capacity of multinary complex hydrides

4. Conclusion

A systematic study of two chemical hydrogen storage systems has been carried out. The first system, polyaniline, was synthesized in its nanostructured forms of nanofibers and nanospheres. This system was investigated for its physisorption of hydrogen through weak secondary atomic bonds. The second main system was investigated for its strong primary atomic bonding of hydrogen and consisted of $LiBH_4$, $LiNH_2$, and MgH_2. Different nano sized additives were added to the complex hydride system, though mainly the complex hydride system was found to destabilize to allow for hydrogen storage at lower temperatures and with faster kinetics. The cumulative results of both the physisorbed and chemisorbed hydrogen storage systems are summarized in Table 1 and Table 2.

Author details

Sesha S. Srinivasan and Prakash C. Sharma
Department of Physics, Tuskegee University, Tuskegee, Alabama, USA

Acknowledgement

5. References

Athawale, A.A. & Bhagwat, S.V.J.J. (2003). Synthesis and characterization of novel copper/polyaniline nanocomposite and application as a catalyst in the Wacker oxidation reaction. *J. Appl. Polymer Science*, Vol. 89, No. 9, 2412-2417

Au, M. (2006). Destabilized and catalyzed alkali metal borohydrides for hydrogen storage with good reversibility, *U.S. Patent Appl. Publ.*, US 2006/0194695 A1, Aug. 31 (2006)

Barkhordarian, G., Klassen, T., Dornheim M., & Bormann, R. (2007). Unexpected kinetic effect of MgB_2 in reactive hydride composites containing complex borohydrides. *J. Alloys Comp.*, Vol. 440, No. 1-2, pp. L18-L21

Bogdanovic, B., & Schwickardi, M. (1997). Ti-doped alkali metal aluminum hydrides as potential novel reversible hydrogen storage materials. *J. Alloys Comp.*, Vol. 253-254, pp. 1-9

Bogdanovic, B., Felderhoff, M., Kaskel, S., Pommerin, A., Schlichte K., & Schuth, F. (2003). Improved hydrogen storage properties of Ti-doped sodium aluminate using titanium nanoparticles as doping agents. *Adv. Mater.*, Vol. 15, No. 12, pp. 1009-1012

Bowman, R.C., & Stetson, N.T. (2010). DOE Hydrogen and Fuel Cells Program Record, On-Board Hydrogen Storage Systems – Projected Performance and Cost Parameters, Record # 9017. www.hydrogen.energy.gov/pdfs/9017_storage_performance.pdf

Broom, D.P. (2011). *Hydrogen Storage Materials; The Characterization of their Storage Properties*, Springer Energy Technology Series, ISBN 978-0-85729-220-9, London, 1st Edition, XII, p. 258

Chen, P., Xiong, Z., Lou, J., Lin J., & Tan, K.L. (2002). Interaction of hydrogen with metal nitrides and imides. *Nature*, Vol. 420, pp. 302-304

Chiou, N-R., Lee, L.J., & Epstein, A.J. (2008). Porous membrane controlled polymerization of nanofibers of polyaniline and its derivatives. *J. Materials Chem.*, Vol. 18, pp. 2085-2089

Cho, S.J., Song, K.S., Kim, J.W., Kim, T.H., & Choo, K. (2002). Hydrogen sorption in HCl treated polyaniline and polypyrrole, new potential hydrogen storage media. *Proceedings of the American Chemical Society, Division of Fuel Chemistry* Vol.47, No.2, pp. 790-791

Cho, S.J., Choo, K., Kim, D.P., & Kim, J.W. (2007). H_2 sorption in HCl-treated polyaniline and polypyrrole. *Catalysis Today*, Vol. 120, No. 3-4, pp. 336-340

Cho, Y.W., Shim J-H., & Lee, B.-J. (2006). Thermal destabilization of binary and complex metal hydrides by chemical reaction: A thermodynamic analysis. *CALPHAD: Computer Coupling of Phase Diagrams and Thermochemistry*, Vol. 30, pp. 65-69, ISSN: 0364-5916

Dehouche, Z., Lafi, L., Grimard, N., Goyette J., & Chahine, R. (2005). The catalytic effect of single-wall carbon nanotubes on the hydrogen sorption properties of sodium alanates. *Nanotechnology*, Vol. 16, pp. 402-409

Dillon, A.C.; Jones, K.M.; Bekkedahl, T.A.; Kiang, C.H.; Bethune, D.S.; & Heben, M.J. (1997) Storage of hydrogen in single-walled carbon Nanotubes, *Nature (London)*, Vol.386, No.6623, pp. 377-379

Ding, H., Wan M., & Wei, Y. (2007). Controlling the Diameter of Polyaniline Nanofibers by Adjusting the Oxidant Redox Potential. *Advanced Materials*, Vol. 19, pp. 465-469

Fichtner, M. (2005). Nanotechnological aspects in materials for hydrogen storage. *Adv. Eng. Mater.*, Vol. 7, pp. 443-455

Fusalba, F., Gouerec, P., Vellers, D., & Belanger, D. (2001). Electrochemical characterization of polyaniline in nonaqueous electrolyte and its evaluation as electrode material for electrochemical supercapacitors. *J. Electrochem. Soc.*, Vol. 148, No. 1, pp. A1-A6

Germain, J., Frechet, J.M.J., & Svec, F. (2007). Hypercrosslinked polyanilines with nanoporous structure and high surface area: potential adsorbents for hydrogen storage. *J. Mater. Chem.*, Vol. 17, No. 47, pp. 4989-4997

Graetz, J., Lee, Y., Reilly, J.J., Park, S., & Vogt, T. (2005). Structures and thermodynamics of the mixed alkali alanates. *Physical Review B: Condensed Matter and Materials Physics*, Vol. 71, No. 18, pp. 184115-184117

Grochala, W., & Edwards, P.P. (2004). Thermal decomposition of the non-interstitial hydrides for the storage and production of hydrogen. *Chem. Rev.*, Vol. 104, pp. 1283-1315

Hu, Y.H., & Ruckenstein, E. (2005). H_2 Storage in Li_3N. Temperature-Programmed Hydrogenation and Dehydrogenation. *Ind. Eng. Chem. Res.*, Vol. 42, No. 21, pp. 5135-5139

Huczko, A. (2000). Template-based synthesis of nanomaterials. *Appl. Phys. A: Materials Science & Processing*, Vol. 70, No. 4, pp. 365-376

Hwang, J.Y., Hwang, S.H., Lee.; Sim, K.S., & Kim, J.W. (2002). Synthesis and hydrogen storage of carbon nanofibers, *Syn. Metals,* Vol.126, No.1, pp. 81-85

Jena, P. (2011). Materials for Hydrogen Storage: Past, Present and Future. *J. Phys. Chem. Lett.,* Vol. 2, No. 3, pp. 206-211

Jensen, C.M., & Zidan, R.A. (2002). Hydrogen storage materials and. method of making by dry homogenation. *U.S. Patent, 6,471935*

Jeon, K.-J., Theodore, A., Wu, C-Y., & Cai, M. (2007). Hydrogen absorption/desorption kinetics of magnesium nano-nickel composites synthesized by dry particle coating technique. *Int. J. Hydrogen Energy,* Vol. 32, No. 12, pp. 1860–1868

Johnson, S.R., Anderson, P.A., Edwards, P.P., Gameson, I., Prendergast, J.W., Al-Mamouri, M., Book, D., Harris, I.R., Speight J.D., & Walton, A. (2005). Chemical activation of MgH_2; a new route to superior hydrogen storage materials. *Chem. Commun.,* pp. 2823-2825

Joo, S.H., Choi, S.J., & Ryoo, R. (2001). Ordered nanoporous arrays of carbon supporting high dispersions of platinum nanoparticles. *Nature,* Vol. 412, No. 6843, pp. 169-172

Jurczyk, M.U., Kumar, A., Srinivasan, S., & Stefanakos, E. (2007). Polyaniline-based nanocomposite materials for hydrogen Storage. *Int. J. Hydrogen Energy,* Vol. 32, No. 8, pp. 1010-1015

Jurczyk, M.U., Srinivasan, S.S., Kumar, A., Goswami, Y., & Stefanakos, E. (2007). Effects of nano catalysts on a $LiBH_4$/$LiNH_2$ system for hydrogen storage. *Proceedings of the MS&T Conference,* Detroit, MI, 2007

Kuritka, I., Negri, F., Brancolini, G., Suess, C., Salaneck, W.R., Friedlein, R. (2006). Lithium intercalation of phenyl-capped aniline dimers: a study by photoelectron spectroscopy and quantum chemical calculations. *J Phys Chem B.,* Vol. 110, No. 38, 19023-19030

Lindino, C.A., Casagrande, M., Peiter, A., & Ribeiro C. (2012). Poly(*o*-methoxyaniline) modified electrode for detection of lithium ions, *Quimica Nova,* ISSN:1678-7064, Vol. 35, No. 3, pp. 449-453

Luo, W. (2004). ($LiNH_2$-MgH_2): a viable hydrogen storage system. *J. Alloys Comp.,* Vol. 381, pp. 284-287

MacDiarmid, A.G., & Epstein, A.J. (1989). Polyanilines: A novel class of conducting polymers. *Faraday Discuss. Chem. Soc.,* Vol. 88, pp. 317-332

McKeown, N.B., Budd, P.M., & Book, D. (2007). Microporous polymers as potential hydrogen storage materials. *Macromol. Rapid Commun.,* Vol. 28, No. 9, pp. 995-1002

Niitani, T., Shimad, M., Kawamura, K., Dokko, K., Rho, Y-H., & Kanamura, K. (2005). Synthesis of Li+ Ion Conductive PEO-PSt Block Copolymer, Electrolyte with Microphase Separation Structure. *Electrochemical & Solid-State Letters,* Vol. 8, pp. A385-A388

Nikitin, A., Li, X., Zhang, Z., Ogasawara, H., Dai, H., & Nilsson, A. (2008). Hydrogen storage in carbon nanotubes through the formation of stable C–H bonds. *Nano Lettters,* Vol. 8, No. 1, pp. 162-167

Orimo, S., Nakamori, Y., Kitahara, G., Miwa, K., Ohba, N., Towata, S., & Zuttel, A. (2005). Dehydrideing and rehydriding reactions of LiBH$_4$. *J. Alloys Comp.*, Vol. 404-406,   pp. 427-430

Panella, B., Kossykh, L., Dettlaff-Weglikowska, U., Hrischer, M., Zerbi, G., & Roth, S. (2005). Volumetric measurement of hydrogen storage in HCl-treated polyaniline and polypyrrole. *Synthetic Metals*, Vol. 151, No. 3, pp. 208-210

Pukhazselvan, D., Gupta, B.K., Srivastava A., & Srivastava, O.N. (2005). Investigations on hydrogen storage behavior of CNT doped NaAlH$_4$. *J. Alloys Compd.*, Vol. 403, pp. 312-317

Rahy, A., & Yang, D.J., Synthesis of highly conductive polyaniline Nanofibers. *Materials Letters*, Vol. 62, pp. 4311-4314

Rivera, L., Srinivasan, S., Matthew, S., Wolan, J., & Stefanakos, E. (2006). Destabilized LiBH$_4$/MgH$_2$ for reversible hydrogen storage. *Proceedings of the AIChE Annual Meeting, Conference Proceedings,* San Francisco, CA, United States, 424d, pp. 6, 2006

Rossberg, K., Paasch, G., & Dunsch, L. (1998). The influence of porosity and the nature of the charge storage capacitance on the impedance behaviour of electropolymerized polyaniline films. *J. Electroanalytical Chem.*, Vol. 443, No. 1, pp. 49-62

Sadek, A.Z., Trinchi, A., Wlodarski, W., Kalantar-zadeh, K., Galatsis, K., Baker, C., & Kaner, R.B. (2005). A room temperature polyaniline nanofiber hydrogen gas sensor. *IEEE Sensors,* Vol. 3, pp. 207-210

Satyapal, S., Petrovic, J., Read, C., Thomas, G., & Ordaz , G. (2007). The U.S. Department of Energy's National Hydrogen Storage Project: Progress towards meeting hydrogen-powered vehicle requirements. *Catalysis Today*, Vol. 120, pp. 246–256

Schlapbach, L., & Zuttel, A. (2001). Hydrogen-storage materials for mobile applications. *Nature,* Vol. 414, No. 15 pp. 353-357

Skowron´ski, J.M.; Urbaniak, J. (2008) Nickel foam/polyaniline-based carbon/palladium composite electrodes for hydrogen storage, Energy Conversion and Management, Vol.49, pp. 2455–2460

Srinivasan, S.S., Niemann, M.U., Goswami, D.Y., Stefanakos, E.K. (2012). Hydrogen-Storage Hydride Complexes, U.S. Patent, 8,153,020, 2012

Srinivasan, S.S., Brinks, H.W., Hauback, B.C., Sun, D., & Jensen, C.M. (2004). Long term cycling behavior of titanium doped NaAlH$_4$ prepared through solvent mediated milling of NaH and Al with titanium dopant precursors. *J. Alloys and Comp.*, Vol. 377, No. 1-2, pp. 283-289

Srinivasan, S., Escobar, D., Jurczyk, M., Goswami, Y., & Stefanankos, E. (2008). Nanocatalyst doping of Zn(BH4)2 for on-board hydrogen storage. *J. Alloys Compd.*, Vol. 462, pp. 294–302

Srinivasan, S., Rivera, L., Stefanakos, E., & Goswami, Y. (2006). Mechano-Chemical Synthesis and Characterization of New Complex Hydrides for Hydrogen Storage, *Mat. Res. Soc. Symp. Proc.,* Vol. 927, pp. EE02

Stefanakos, E.K., Goswami, D.Y., Srinivasan, S.S., & Wolan, J. (2007). Hydrogen Energy, Kutz, Myer (Hrsg.) *Environmentally Conscious Alternative Energy Production, John Wiley & Sons,* 4th volume, Chapter 7, pp. 165

Stejskal, J., Kratochvil, P., & Jenkins A.D. (1996). The formation of polyaniline and the nature of its structures. *Polymer,* Vol. 37, No. 2, pp. 367-369

Stejskal, J., & Gilbert, R.G. (2002). Polyaniline. Preparation of a conducting polymer (IUPAC Technical Report). *Pure and App. Chem.,* Vol. 74, pp. 857-867

Trivedi, D.C. (1997). Polyanilines. *Handbook of Organic Conductive Molecules and Polymers,* H.S. Nalwa (Ed.) Wiley, Chichester, UK 2, pp. 505-572

US Department of Energy. (2003). Report of the Basic Energy Science Workshop on Hydrogen Production, Storage and use prepared by Argonne National Laboratory, May 13-15, (2003)

Vajo, J.J., Skeith, E., & Mertens, F. (2005). Reversible Storage of Hydrogen in Destabilized LiBH$_4$. *J. Phys. Chem. B,* Vol. 109, pp. 3719-3722

Virji, S., Kaner, R.B., & Weiller, B.H. (2006). Hydrogen sensors based on conductivity changes in polyaniline nanofibers. *J. Phys. Chem.* B, Vol. 110, No. 44, pp. 22266-22270

Wang, Y., & Jing, X.J. (2008). Synthesis and hydrogen storage of carbon nanofibers. Synthetic Metals. *J. Phys. Chem. B,* Vol. 112, No. 4, pp. 1157-1162

Wu, C.Z., Wang, P., Yao, X., Liu, C., Chen, C.M., Lu G.Q., & Cheng, H.M. (2006). Hydrogen storage properties of MgH$_2$/SWNT composite prepared by ball milling. *J. Alloys Comp.,* Vol.420, pp. 278-282

Yang, Y., Ouyang, J., Ma, L., Tseng, R.J., & Chu, C.-W. (2006). Electrical Switching and Bistability in Organic/Polymeric Thin Films and Memory Devices. *Adv. Funct. Mater.,* Vol. 16, No. 8, pp. 1001-1014

Yao, X., Wu, C.Z., Wang, H., Cheng, H.M., Lu, G.Q. (2006). Effects of Carbon Nanotubes and Metal Catalysts on Hydrogen Storage in Magnesium Nanocomposites. *J. Nanoscience and Nanotechnology,* Vol. 6, No. 2, pp. 494-498, ISSN 1533-4880, Online ISSN: 1533-4899

Yildirim, T., & Ciraci, S. (2005). Titanium-Decorated Carbon Nanotubes as a Potential High-Capacity Hydrogen Storage Medium. *Phys. Rev. Lett.,* Vol. 94, pp. 175501-175504

Yu, X.B., Grant D.M., & Walker, G.S. (2006). A new dehydrogenation mechanism for reversible multicomponent borohydride systems—The role of Li–Mg alloys. *Chem. Commun.,* pp. 3906-3908

Yvon, K., & Bertheville, B. (2006). Magnesium based ternary metal hydrides containing alkali and alkaline-earth elements. *J. Alloys Comp.,* Vol. 425, pp. 101-108

Zaluska, A., Zaluski, L ., & Strom-Olsen, J.O. (2001). Structure, catalysis and atomic reactions on the nano-scale: a systematic approach to metal hydrides for hydrogen storage. *Appl. Phys. A,* Vol. 72, pp. 157-165

Zhang, D., & Wang, Y. (2006). Synthesis and applications of one dimensional nano-structured polyaniline: An overview. *Mater. Sci. and Engg. B,* Vol. 134, No. 1, pp. 9-19

Zhang, G., Li, X., Jia, H., Pang, X., Yang, H., Wang, Y., & Ding, K. (2012). Preparation and Characterization of Polyaniline (PANI) doped-Li$_3$V$_2$(PO$_4$)$_3$. *Int. J. Electrochem. Sci.,* Vol. 7, pp. 830-843

Zuttel, A. (2004). Hydrogen Storage Methods. *Die Naturwissenschaften,* Vol. 91, pp. 157-172

Zuttel, A., Wenger, P., Rentsch, S., Sudan, P., Mauron Ph., & Emmeneger, Ch. (2003). LiBH$_4$ a new hydrogen storage material. *J. Power Sources,* Vol. 118, pp. 1-7